Angewandte Chemie
Eine Zeitschrift der Gesellschaft Deutscher Chemiker

Supporting Information

Magnetic Anisotropy in Divalent Lanthanide Compounds

Weibing Zhang, Almas Muhtadi, Naoya Iwahara, Liviu Ungur, and Liviu F. Chibotaru**

anie_202003399_sm_miscellaneous_information.pdf

Supporting Information

Computational details

The geometry of all investigated complexes was optimized by unrestricted DFT using B3LYP functional. The equilibrium Ln-O distance is indicated in Figs. 1 and 3-5. The *ab initio* calculations of RASSCF/ RASPT2/ RASSI/ SINGLE_ANISO level were carried out within the MOLCAS package.[1] All atoms were described by quadruple-zeta ANO-RCC basis sets.[2] In this approach, relativistic corrections are included via the Douglas-Kroll-Hess formalism, in two steps.[3] In the first step, scalar corrections are included in the basis sets used for the expansion of the molecular orbitals of the corresponding eigenstates at RASSCF level. Spin-orbit coupling is included in the second step (RASSI), using the obtained RASSCF states as input.[3d, 4] In this approach, spin-orbit interaction in described by an effective mean-field operator (AMFI). Electronic correlation was considered within multiconfigurational second-order perturbation theory (RASPT2).[1a, 3f, 5] For the neutral LnO molecules, the active space of the RASSCF method included the [$5p^6$ $4f^N$ $6s^1$ $5d^0$] shells of the lanthanide, where is the corresponding number of electrons in the 4*f* shell of the Ln^{3+}. In order to reduce the computational cost of these calculations, the $5d^0$ shell was included in RAS3 space, allowing all configurations with maximum two electrons in this space. The $2p^6$ orbitals of the oxygen were always doubly occupied. This is consistent with unrestricted-DFT results, which also showed that the unpaired spins are located in the 4*f* and 6*s* shells of the lanthanide, while the oxygen contained no spin density. All attempts to include the $2p^6$ shell in the active space were not successful, as they were replaced by metal's orbitals of either $4d^{10}$ or $5p^6$ kind. The spin-orbit interaction included: ^{8}F and ^{6}F terms for TbO; ^{7}H, ^{7}F, ^{5}H and ^{5}F terms for DyO; ^{6}I, ^{6}F, ^{6}S, ^{4}I, ^{4}F and ^{4}S terms for HoO. For the (re)calculation of $[DyO]^+$,[9] the active space included the [$5p^6$ $4f^N$ $5d^0$] orbitals of the metal site, with $5d^0$ shell included in RAS3 space. As in the case of neutral LnO molecules, the oxigen's $2p^6$ shell was not favored in the active space because its presence there was not leading to a significant lowering of the total energy: the oxygen's $2p^6$ shell is replaced by other metal's orbitals in the process of orbital optimization. For the study of the neutral DyO deposited on the hexagonal boron-nitride (h-BN) surface, geometry optimization was carried out by non-periodic DFT calculations with ORCA quantum chemistry package,[6] using BP86 density functional, def2-TZVP basis sets for all atoms,[7] tight convergence thresholds, Grimme's atom-pairwise dispersion correction with the Becke-Johnson damping scheme (D3BJ),[8] and grid7 as computational options.

Computational results

DOI: 10.1002/anie.2016XXXXX

Table S1. Low-lying doublets in [TbO]

KD	Energy (cm^{-1})		$\|m_J\|$	M (μ_B)	Weight (%) (CASPT2/RASSI)		Exp. (cm^{-1})
	CASSCF / RASSI	CASPT2 / RASSI			S=7/2	S=5/2	Ref.[10a]
1	0	0	13/2	10.01	100.00	0.00	0
2	341	351	11/2	8.18	99.24	0.75	355
3	710	735	9/2	6.35	98.53	1.46	750
4	1108	1153	7/2	4.54	97.98	2.01	1183
5	1535	1607	5/2	2.75	97.65	2.34	1624
6	1656	1784	11/2	8.28	29.50	70.49	1654
7	1981	2095	3/2	1.05	97.68	2.31	2101
8	2086	2229	9/2	6.52	33.24	66.75	2160
9	2386	2571	1/2	0.26	98.64	1.35	2610
10	2521	2687	7/2	4.80	42.15	57.84	-
11	2675	2746	11/2	8.56	71.25	28.74	2900
12	2923	3086	9/2	6.65	67.23	32.77	3118
13	2990	3119	5/2	3.19	58.68	41.32	3188
14	3127	3291	1/2	1.38	90.86	9.13	-
15	3181	3405	3/2	2.00	79.55	20.44	-
16	3322	3451	7/2	4.74	58.84	41.15	-
17	3677	3846	5/2	2.91	43.37	56.62	-
18	4063	4208	1/2	0.76	90.67	9.32	-
19	4087	4287	3/2	1.25	27.24	72.75	-
20	4089	4288	9/2	7.00	26.02	73.97	-

Table S2. Low-lying doublets in [DyO]

ID	Energy (cm^{-1})		$\|m_J\|$	M (μ_B)	Weight (%) (CASPT2/RASSI)		Exp. (cm^{-1})
	CASSCF / RASSI	CASPT2 / RASSI	CASPT2 / RASSI		S=3	S=2	Ref.[10b]
1	0	0	8	11.01	100.00	0.00	0
2	626	761	7	9.24	96.50	3.49	770
3	1254	1515	6	7.61	96.27	3.72	1630
4	1561	2178	5	6.22	97.59	2.40	1683
5	1808	2258	7	9.30	31.54	68.45	2420
6	2208	2624	4	5.10	99.19	0.80	-
7	2277	2739*	0	--	99.99	0.00	-
8	2423	2757	1	1.44	99.99	0.00	-
9	2504	2793	3	4.04	99.91	0.08	-
10	2524	2795	2	2.81	99.99	0.00	-
11	2526*	3036	6	7.86	47.81	52.18	-
12	2830	3605	5	6.42	60.48	39.51	-
13	3221	3972	4	5.06	62.18	37.81	-
14	3472	4166	7	9.28	71.41	28.58	-
15	3603	4197	3	3.96	56.29	43.70	-
16	3652	4307	2	2.54	47.80	52.19	-
17	3663*	4359	1	1.27	43.03	56.96	-
18	3789	4367*	0	--	41.18	58.81	-
19	4209	4728	6	7.66	55.06	44.93	-
20	4639	5317	5	6.03	42.96	57.03	-
21	4857	5575	6	8.01	54.02	45.97	-

* -- singlet state

Table S3. Low-lying doublets in [HoO]

SUPPORTING INFORMATION

KD	Energy (cm^{-1})		$\|m_J\|$	M (μ_B)	Weight (%) (CASPT2/RASSI)		Exp. (cm^{-1})
	CASSCF / RASSI	CASPT2 / RASSI			S=5/2	S=3/2	Ref.[10c]
1	0	0	17/2	11.01	100.00	0.00	0
2	464	673	15/2	9.31	84.91	15.08	609
3	796	1218	13/2	8.13	96.39	3.60	1130
4	984	1364	15/2	9.37	36.32	63.67	-
5	1096	1448	11/2	6.99	99.26	0.73	-
6	1130	1546	9/2	5.75	99.75	0.24	-
7	1175	1612	7/2	4.46	99.83	0.16	-
8	1238	1679	5/2	3.16	99.84	0.15	-
9	1285	1744	3/2	1.87	99.89	0.10	-
10	1311	1788	1/2	0.62	99.98	0.01	1861
11	1607	2056	13/2	7.93	31.28	68.71	-
12	1859	2392	11/2	6.66	28.09	71.90	-
13	1995	2527	9/2	5.46	25.91	74.08	-
14	2087	2602	7/2	4.25	25.01	74.98	-
15	2163	2680	5/2	3.03	24.88	75.11	-
16	2225	2760	3/2	1.82	25.47	74.52	-
17	2260	2812	1/2	0.61	26.24	73.75	-

Table S4. Low-lying doublets in [DyO] deposited on hexagonal-BN

ID	Energy (cm^{-1})		$\|m_J\|$ **	M (μ_B)	Weight (%) (CASPT2/RASSI)	
	CASSCF / RASSI	CASPT2 / RASSI			S=3	S=2
1	0	0	8	11.01	99.99	0.00
2	560	697	7	9.22	92.71	7.28
3	1084	1397	6	7.63	93.38	6.61
4	1517	1718	8	9.26	25.54	74.45
5	1675	1994	5	6.26	96.06	3.93
6	1812	2386	4	5.07	98.62	1.37
7	1968	2508	6	7.78	35.33	64.66
8	2003*	2525*	1	---	99.26	0.73
9	2046	2547		4.83	99.84	0.15
10	2084	2607		8.24	99.95	0.04
11	2250	2635		10.38	99.96	0.03
12	2695	3082	5	6.44	41.29	58.70
13	3011	3473	4	5.06	41.79	58.20
14	3206	3705	3	3.59	37.68	62.31
15	3289*	3775*	0	---	31.74	68.25
16	3329	3817		5.96	31.68	68.31
17	3407	3875		8.49	31.54	68.45
18	3749	3964	7	9.53	81.75	18.24
19	4150	4397	6	7.74	69.54	30.45
20	4534	4844	5	6.08	60.02	39.97
21	4822	5102	6	7.85	41.36	58.63

* -- singlet state

** -- m_J values are not entirely valid in the absence of rotational symmetry

Red color denotes the doublet states which have main anisotropy axis oriented in the perpendicular direction with respect to the main quantization axis of the ground doublet state.

Analysis of molecular multiplets in [LnO]

The obtained spectrum of multiplets differs from the one arising in trivalent lanthanide complexes. In the latter the molecular multiplets are merely split atomic $^{2S+1}L_J$ multiplets, gathered in groups of levels belonging to neighbor *J*-multiplets which arise from the same term ^{2S+1}L. As an example, the two groups of low-lying multiplets in $[DyO]^+$ originate from the atomic multiplets $^6H_{15/2}$ and $^6H_{13/2}$, respectively (Fig. S2). In the case of divalent lanthanide complexes, the molecular multiplets originate from atomic multiplets as well, however, the order of the latter in the spectrum differs drastically from Ln^{3+}. As usual, the ground atomic multiplet $^{2S+1}L_J$ originates from a *LS* term of Hund type, corresponding to the addition of the spin $S-1/2$ of the ground term of the $4f^N$ shell to the spin 1/2 of one electron in the 6*s* orbital. Since this orbital does not possess orbital momentum, *L* is the same as in the ground term of the configuration $4f^N$ (i.e., of the ion Ln^{3+}). However, at variance to the Ln^{3+} ions, the next atomic multiplet does not originate from the same term *LS* as the ground one but arises from the non-Hund term $LS-1$ in which the $S-1/2$ spin of the $4f^N$ shell couples antiferromagnetically to the spin 1/2 of the electron in the 6*s* orbital. Due to the reversal of one spin, the total angular momentum is reduced in this multiplet by unity with respect to the ground multiplet, $^{2S-1}L_{J-1}$. The next (second excited) atomic multiplet follows the "normal order", i.e., originates from the ground term *LS* and corresponds to a total angular momentum by one unit less than the ground multiplet, $^{2S+1}L_{J-1}$. The fact that the non-Hund atomic multiplet (the first excited) intrudes between the two Hund multiplets is

entirely due to the smallness of intra-atomic exchange interaction between 6*s* and 4*f* orbitals. This is the consequence of the large radius of the 6*s* orbitals resulting in a Hund splitting of the atomic terms to ca 2000 cm^{-1} (Fig. S1), which is significantly smaller than the spin-orbit separation of the atomic multiplets.

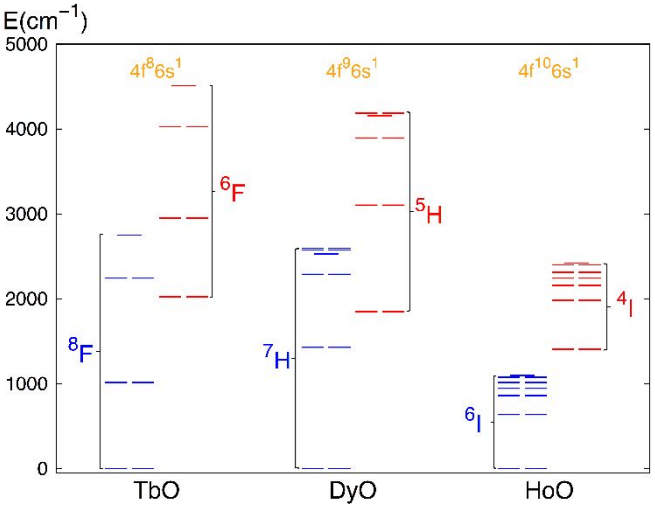

Figure S1. Low-lying molecular terms of [LnO] for Ln=Tb, Dy and Ho. The curly braces indicate the levels originating from a given atomic term $^{2S+1}$L of Ln^{2+}. The orbital configuration containing magnetic electrons is shown in the top for each complex.

In the case of [TbO] and [DyO] the split *J*-multiplets overlap at a large extent as consequence of intruded non-Hund multiplet between the lowest Hund ones as discussed above. This is testified by numbers in parentheses in the first column of Tables S1 and S2 denoting the parent atomic multiplet. In the case of [HoO] the groups of levels belonging to different multiplets do not overlap because of smaller crystal-field splitting due to more contracted 4*f* orbitals in Ho^{2+}. The spin-orbit multiplets and the corresponding energy levels originating from different terms mix with each other due to both intra-atomic *J*−*J* mixing and crystal-field effect, the latter being much stronger (e.g. ^6I and ^4I in the case of $[HoO]^0$).
Indeed, Tables S1-S3 show that various multiplets nominally assigned to one atomic term have very different weights of the two lowest atomic terms (denoted in the tables by their spins). In the case of [HoO] the mixture of different terms in multiplet wave functions is significantly smaller (see Table S3) due to much weaker crystal field as discussed above.

Analysis of molecular multiplets in $[DyO]^+$

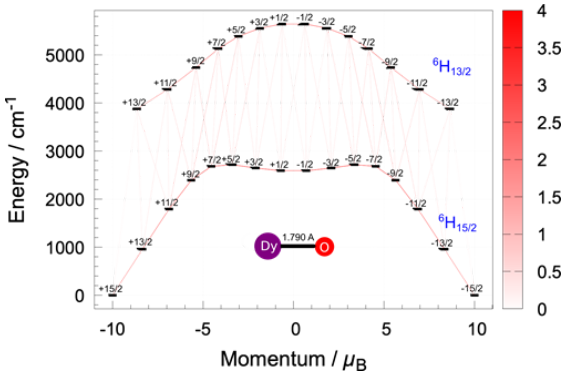

Figure S2. Multiplet spectrum and magnetization blocking barrier for $[DyO]^+$ calculated within the same level of the theory as the compounds [LnO] in Fig. 1 (legend for colour and lines similar to Fig. 1).

As shown in Fig. S2, the two low-lying groups of multiplets originate from the ground atomic ^6H term of Dy^{3+}, the lower group arising from the atomic $^6H_{15/2}$ multiplet and the higher one from the $^6H_{13/2}$ multiplet. Given the axial symmetry of the complex the projection of the total momentum J on the Dy-O axis is exactly conserved. As a result, the ground doublet ±15/2 is of net $^6H_{15/2}$ origin, while doublets with lower $|M_J|$ arise from the mixture of $^6H_{15/2}$ and the $^6H_{13/2}$ states (red vertical lines in Fig. S2).

Composition of active orbitals

Table S5. Composition of RASSCF state-averaged molecular orbitals of TbO, S=7/2 (weights)

Orbital number	33	34	35	36	37	38	39	40
Tb 5s	0.000	0.000	0.000	0.000	0.000	0.000	0.001	0.001
Tb 6s	0.000	0.000	0.000	0.000	0.000	0.000	0.000	0.797
Tb 5p	0.000	0.000	0.000	0.000	0.000	0.000	0.002	0.001
Tb 6p	0.000	0.000	0.000	0.000	0.000	0.000	0.000	0.134
Tb 5d, |m|=2	0.000	0.000	0.000	0.000	0.000	0.000	0.000	0.000
Tb 5d, |m|=1	0.003	0.003	0.000	0.000	0.000	0.000	0.000	0.000
Tb 5d, |m|=0	0.000	0.000	0.000	0.000	0.000	0.000	0.007	0.038
Tb 4f, |m|=3	0.000	0.000	0.999	0.999	0.000	0.000	0.000	0.000
Tb 4f, |m|=2	0.000	0.000	0.000	0.000	0.999	0.999	0.000	0.000
Tb 4f, |m|=1	0.994	0.994	0.000	0.000	0.000	0.000	0.000	0.000
Tb 4f, |m|=0	0.000	0.000	0.000	0.000	0.000	0.000	0.987	0.000
O 2s	0.000	0.000	0.000	0.000	0.000	0.000	0.001	0.001
O 2p, |m|=1	0.004	0.004	0.000	0.000	0.000	0.000	0.000	0.000
O 2p, |m|=0	0.000	0.000	0.000	0.000	0.000	0.000	0.008	0.001
Total	1.002	1.002	0.999	0.999	0.999	0.999	1.007	0.973

Table S6. Composition of RASSCF state-averaged molecular orbitals of DyO, S=3 (weights)

Orbital number	33	34	35	36	37	38	39	40
Dy 5s	0.000	0.000	0.000	0.000	0.000	0.000	0.001	0.001
Dy 6s	0.000	0.000	0.000	0.000	0.000	0.000	0.000	0.798
Dy 5p	0.000	0.000	0.000	0.000	0.000	0.000	0.002	0.001
Dy 6p	0.000	0.000	0.000	0.000	0.000	0.000	0.000	0.120
Dy 5d, |m|=2	0.000	0.000	0.000	0.000	0.000	0.000	0.000	0.000
Dy 5d, |m|=1	0.003	0.003	0.000	0.000	0.000	0.000	0.000	0.000
Dy 5d, |m|=0	0.000	0.000	0.000	0.000	0.000	0.000	0.006	0.037
Dy 4f, |m|=3	0.000	0.000	0.999	0.999	0.000	0.000	0.000	0.000
Dy 4f, |m|=2	0.000	0.000	0.000	0.000	0.999	0.999	0.000	0.000
Dy 4f, |m|=1	0.994	0.994	0.000	0.000	0.000	0.000	0.000	0.000
Dy 4f, |m|=0	0.000	0.000	0.000	0.000	0.000	0.000	0.987	0.000
O 2s	0.000	0.000	0.000	0.000	0.000	0.000	0.001	0.001
O 2p, |m|=1	0.005	0.005	0.000	0.000	0.000	0.000	0.000	0.000
O 2p, |m|=0	0.000	0.000	0.000	0.000	0.000	0.000	0.008	0.002
Total	1.002	1.002	0.999	0.999	0.999	0.999	1.007	0.961

Table S7. Composition of RASSCF state-averaged molecular orbitals of HoO, S=5/2 (weights).

Orbital number	33	34	35	36	37	38	39	40
Ho 5s	0.000	0.000	0.000	0.000	0.000	0.000	0.001	0.001
Ho 6s	0.000	0.000	0.000	0.000	0.000	0.000	0.000	0.806
Ho 5p	0.000	0.000	0.000	0.000	0.000	0.000	0.002	0.000
Ho 6p	0.000	0.000	0.000	0.000	0.000	0.000	0.000	0.144
Ho 5d, |m|=2	0.000	0.000	0.000	0.000	0.000	0.000	0.000	0.000
Ho 5d, |m|=1	0.002	0.002	0.000	0.000	0.000	0.000	0.000	0.000
Ho 5d, |m|=0	0.000	0.000	0.000	0.000	0.000	0.000	0.006	0.042
Ho 4f, |m|=3	0.000	0.000	0.999	0.999	0.000	0.000	0.000	0.000

Ho 4f, |m|=2	0.000	0.000	0.000	0.000	0.999	0.999	0.000	0.000
Ho 4f, |m|=1	0.994	0.994	0.000	0.000	0.000	0.000	0.000	0.000
Ho 4f, |m|=0	0.000	0.000	0.000	0.000	0.000	0.000	0.988	0.000
O 2s	0.000	0.000	0.000	0.000	0.000	0.000	0.001	0.001
O 2p, |m|=1	0.005	0.005	0.000	0.000	0.000	0.000	0.000	0.000
O 2p, |m|=0	0.000	0.000	0.000	0.000	0.000	0.000	0.008	0.002
Total	1.001	1.001	0.999	0.999	0.999	0.999	1.005	0.996

Table S8. Composition of RASSCF state-averaged molecular orbitals of DyO/BN, S=3 (weights).

Orbital number	**204**	**205**	**206**	**207**	**208**	**209**	**210**	**211**
Dy 5s	0.000	0.000	0.000	0.000	0.000	0.000	0.001	0.001
Dy 6s	0.000	0.000	0.000	0.000	0.000	0.000	0.000	0.782
Dy 5p	0.000	0.000	0.000	0.000	0.000	0.000	0.001	0.000
Dy 6p	0.000	0.000	0.000	0.000	0.000	0.000	0.000	0.169
Dy 5d, |m|=2	0.000	0.000	0.000	0.000	0.000	0.002	0.004	0.050
Dy 5d, |m|=1	0.000	0.000	0.000	0.000	0.002	0.000	0.001	0.005
Dy 5d, |m|=0	0.000	0.000	0.000	0.000	0.000	0.000	0.001	0.002
Dy 4f, |m|=3	0.082	0.024	0.039	0.416	0.025	0.874	0.527	0.000
Dy 4f, |m|=2	0.056	0.408	0.871	0.002	0.484	0.071	0.102	0.000
Dy 4f, |m|=1	0.860	0.032	0.089	0.469	0.201	0.049	0.294	0.000
Dy 4f, |m|=0	0.001	0.536	0.000	0.112	0.285	0.000	0.065	0.000
O 2s	0.000	0.000	0.000	0.000	0.000	0.000	0.001	0.000
O 2p, |m|=1	0.000	0.000	0.000	0.000	0.000	0.004	0.006	0.001
O 2p, |m|=0	0.000	0.000	0.000	0.000	0.004	0.000	0.000	0.000
Total	0.999	1.000	0.999	0.999	1.001	1.000	1.003	1.010

Crystal field and orbital energy levels

The relation between the crystal field for the *f*-shell and that for the ground *LS*-term is derived. On this basis, the *f* orbital energy levels are calculated.

Crystal fields for the ground LS-term and the f-shell ---

Suppose the crystal-field comes from the energy splitting of the *f* orbitals. The crystal-field describing the latter is written as

$$\hat{H}_{CF} = \sum_{kq} b_{kq} \hat{o}_{kq} , \qquad (1)$$

where $\hat{o}_{kq}$ is irreducible tensor operator of rank *k* (component *q*) acting on the *f*-shell,

$$\hat{o}_{kq} = \sum_{mm'\sigma} \frac{C^{lm}_{lm'kq}}{C^{l}_{llk0}} \hat{c}^{\dagger}_{m\sigma} \hat{c}_{m'\sigma} , \qquad (2)$$

$l = 3$, $C^{c\gamma}_{a\alpha b\beta}$ are Clebsch-Gordan coefficients [11], $\hat{c}^{\dagger}_{m\sigma}$ ($\hat{c}_{m\sigma}$) is electron creation (annihilation) operator in orbital $m\sigma$, and b_{kq} is the crystal-field parameter for the *f*-shell. The product of the creation and annihilation operators is expressed by the Racah's irreducible tensor operator $\hat{U}^{(k)}_{q}$ acting on the space of f^n configurations [12]:

$$\sum_{\sigma} \hat{c}^{\dagger}_{m\sigma} \hat{c}_{m'\sigma} = \sum_{kq} (-1)^{l-m'} \sqrt{2k+1} C^{kq}_{lml-m'} \hat{U}^{(k)}_{q} . \qquad (3)$$

Substituting Eqs. (2) and (3) into Eq. (1), and using the symmetry and unitarity of Clebsch-Gordan coefficients,

$$\hat{H}_{CF} = \sum_{kq} b_{kq} \frac{\sqrt{2k+1}}{C^{k0}_{lll-l}} \hat{U}^{(k)}_{q} . \qquad (4)$$

The CF Hamiltonian for the high-spin $f^n s^1$ states (n = 8, 9, 10),

$$|f^n s^1, LM_L SM_S\rangle = \sum_{m_S\sigma} |f^n s^1, L_f M_L S_f m_S, s\sigma\rangle \; C^{SM_S}_{S_f m_S s\sigma} , \qquad (5)$$

is derived by projecting $\hat{U}_q^{(k)}$ into the space of the ground *LS*-term states. Here, the ket in the right hand side is decoupled state, the left is coupled, L_f and S_f are the angular momenta for the ground *LS*-term of the f^n, $s = 1/2$. Substituting Eq. (5) into

$$\hat{U}_q^{(k)} = \sum_{M_L M_L' M_S} \langle f^n s^1,\ LM_L SM_S | \hat{U}_q^{(k)} | f^n s^1,\ LM_L' SM_S \rangle \ | f^n s^1,\ LM_L SM_S \rangle \ \langle f^n s^1,\ LM_L' SM_S |$$

and applying Wigner-Eckart theorem [11],

$$\hat{U}_q^{(k)} = \sum_{M_L M_L' M_S} \frac{\langle f^n,\ ^{2S_f+1}L \,||\, \hat{U}^{(k)} \,||\, f^n,\ ^{2S_f+1}L \rangle}{\sqrt{2L+1}} C^{LM_L}_{LM_L' kq} | f^n s^1,\ LM_L SM_S \rangle \ \langle f^n s^1,\ LM_L' SM_S | \ . \qquad (6)$$

Furthermore, using the irreducible tensor operator acting on $|f^n,\ LM_L\rangle$,

$$\hat{O}_{kq} = \sum_{M_L M_{L'}} \frac{C^{LM_L}_{LM_{L'} kq}}{C^{LL}_{LLk0}} | f^n,\ LM_L \rangle \ \langle f^n,\ LM_{L'} | \ ,$$

Eq. (4) is expressed as

$$\hat{H}_{CF} = \sum_{kq} b_{kq} \frac{C^{k0}_{LL-I}}{C^{k0}_{III-I}} \ \langle f^n,\ ^{2S_f+1}L \,||\, \hat{U}^{(k)} \,||\, f^n,\ ^{2S_f+1}L \rangle \ \hat{O}_{kq} \ . \qquad (7)$$

From this expression, the CF parameters defined by

$$\hat{H}_{CF} = \sum_{kq} B_{kq} \hat{O}_{kq} \ , \qquad (8)$$

and b_{kq} have the following relation:

$$B_{kq} = b_{kq} \frac{C^{k0}_{LL-I}}{C^{k0}_{III-I}} \ \langle f^n,\ ^{2S_f+1}L \,||\, \hat{U}^{(k)} \,||\, f^n,\ ^{2S_f+1}L \rangle \ . \qquad (9)$$

From this expression, b_{kq} are derived. The reduced matrix elements of Racah's $\hat{U}^{(k)}$ are tabulated in Ref. [13]. The matrix elements for Tb (L = 3, S = 3), Dy (L = 5, S = 5/2), and Ho (L = 6, S = 2) are shown in Table S9.

Table S9. The reduced matrix elements of Racah's $\hat{U}^{(k)}$.

	Tb (L = 3, S = 3)	Dy (L = 5, S = 5/2)	Ho (L = 6, S = 2)
k = 2	+1	$\frac{1}{3}\sqrt{\frac{143}{14}}$	$-\sqrt{\frac{13}{66}}$
k = 4	+1	$-\frac{2}{3}\sqrt{\frac{13}{7}}$	$-\frac{\sqrt{442}}{33}$
k = 6	+1	$-\frac{1}{3}\sqrt{\frac{85}{7}}$	$\frac{5}{11}\sqrt{\frac{323}{21}}$

Orbital splitting ---

B_{kq} in Eq. (8) for the high-spin LS-terms are calculated at CASSCF and CASSCF/XMS-CASPT2 levels. Although the maximum *k* for Dy and Ho is larger than 6, the higher rank terms are weak (a few % in energy). Thus, the higher rank terms are ignored. From Eq. (9), b_{kq} for the Hund states (Table S10) and orbital splittings (eigenvalues of Eq. (1). Table S11) are calculated. Since the system has $C_{\infty h}$ symmetry, b_{kq} is nonzero when *q* = 0.

The ground and first excited CASSCF states are characterized by maximum $|M_L| = L$ and $|M_L| = L - 1$, respectively. The gaps between them for Dy, Ho are, within one-electron picture, the energy gaps $\varepsilon_1 - \varepsilon_2 = 1424$, $\varepsilon_0 - \varepsilon_1 = 769$, respectively, which agree well with the CASSCF energy gaps.

The same procedure has been applied to DyO/BN. The calculated b_{kq} are listed in Table S12.

Table S10. b_{kq} (cm^{-1}).

k	*q*	Tb	Dy	Ho

		CASSCF	CASPT2	CASSCF	CASPT2	CASSCF	CASPT2
2	0	-1643.81	-1830.26	-1512.05	-1580.29	-1870.16	-2377.05
4	0	152.192	188.477	236.304	391.097	162.934	302.155
6	0	-0.642094	1.52915	-5.38604	-9.11512	-3.52992	-8.58072

Table S11. Orbital energy levels of isolated LnO and DyO/BN (cm^{-1}). "Orbital" indicates the active orbitals in Fig. S3.

$\|m\|$	Orbital	Tb		Dy		Ho		$\|m\|$	Orbital	DyO/BN
		CASSCF	CASPT2	CASSCF	CASPT2	CASSCF	CASPT2			CASSCF
3	35, 36	0	0	0	0	0	0	3	35 (36)	0
2	37, 38	1141	1191	762	340	1352	1430	3	36 (35)	20
1	33, 34	2520	2824	2186	2140	2834	3482	2	37 (38)	726
0	39	3125	3451	3071	3427	3603	4761	2	38 (37)	743
								1	33 (34)	1919
								1	34 (33)	2071
								0	39	2710

Table S12. b_{kq} for DyO/BN (cm^{-1})

k	q	b_{kq}	k	q	b_{kq}
2	0	-1348.94	6	0	-3.34673
	±1	±18.0616 + 17.9202 *i*		±1	±0.502085 + 0.501075 *i*
	±2	-1.05988 ∓ 62.7121 *i*		±2	∓0.49144 *i*
4	0	195.464		±3	±0.347458 - 0.350839 *i*
	±1	±4.48691 + 4.4332 *i*		±4	-0.270435 ± 0.010566 *i*
	±2	-0.0244623 ± 1.89568 *i*		±5	∓0.277957 - 0.2579 *i*
	±3	∓0.512909 + 0.529606 *i*		±6	0.0134459 ± 0.379229 *i*
	±4	-5.46252 ± 0.157032 *i*			

Active orbitals

Orbital	Moment	Spin S=7/2	Spin S=5/2

33	±1	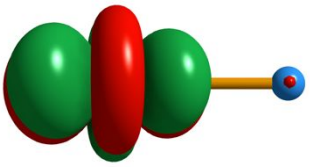	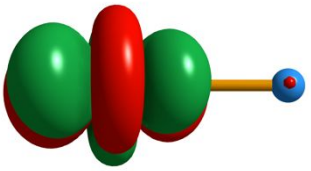
34		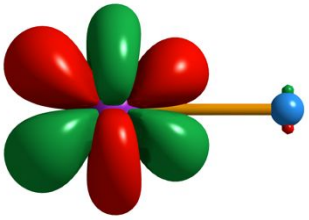	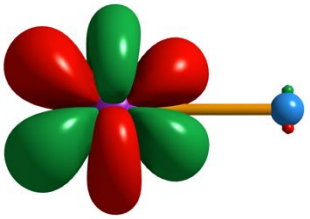
35	± 3	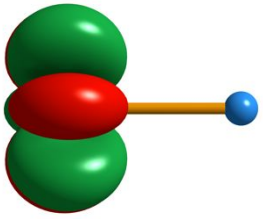	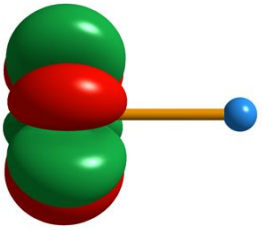
36		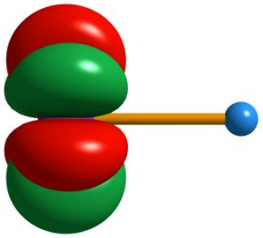	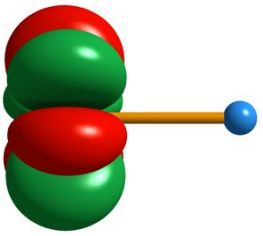
37	± 2	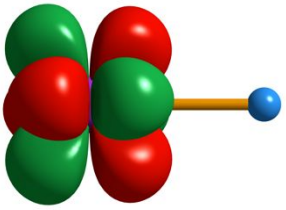	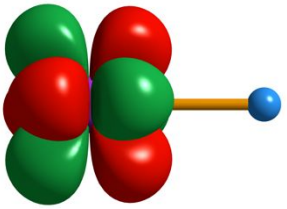
38		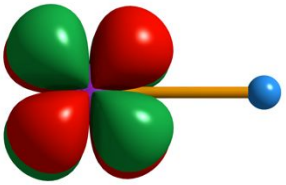	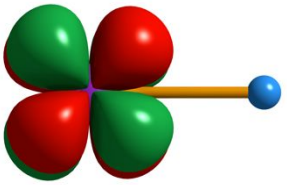

39	0	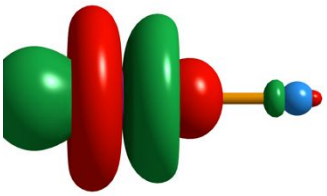	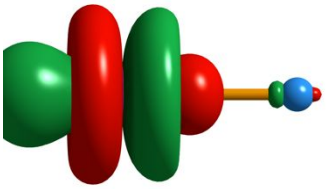
40	6s	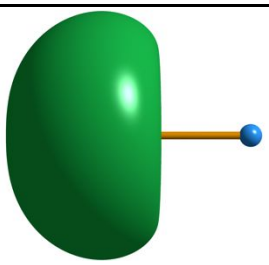	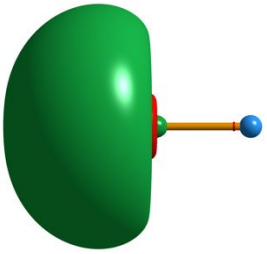

Figure S3. Active orbitals bearing the magnetic electrons in the ground multiplets of the Hund and the first excited non-Hund terms, respectively, of the [TbO] compound. [All orbitals are of the Tb(II) type, hence the orbitals are mainly localized on the Tb site.

References:

[1] a) F. Aquilante, J. Autschbach, R. K. Carlson, L. F. Chibotaru, M. G. Delcey, L. De Vico, I. F. Galvan, N. Ferre, L. M. Frutos, L. Gagliardi, M. Garavelli, A. Giussani, C. E. Hoyer, G. Li Manni, H. Lischka, D. X. Ma, P. A. Malmqvist, T. Muller, A. Nenov, M. Olivucci, T. B. Pedersen, D. L. Peng, F. Plasser, B. Pritchard, M. Reiher, I. Rivalta, I. Schapiro, J. Segarra-Marti, M. Stenrup, D. G. Truhlar, L. Ungur, A. Valentini, S. Vancoillie, V. Veryazov, V. P. Vysotskiy, O. Weingart, F. Zapata, R. Lindh, *J. Comput. Chem.* **2016**, *37*, 506-541; b) L. F. Chibotaru, L. Ungur, *J. Chem. Phys.* **2012**, *137*.

[2] a) B. O. Roos, R. Lindh, P. A. Malmqvist, V. Veryazov, P. O. Widmark, A. C. Borin, *J. Phys. Chem. A* **2008**, *112*, 11431-11435; b) B. O. Roos, V. Veryazov, P. O. Widmark, *Theor. Chem. Acc.* **2004**, *111*, 345-351.

[3] a) M. Douglas, N. M. Kroll, *Ann. Phys.* **1974**, *82*, 89-155; b) B. A. Hess, *Phys. Rev. A* **1986**, *33*, 3742-3748; c) M. Reiher, *Wires Comput. Mol. Sci.* **2012**, *2*, 139-149; d) P. A. Malmqvist, B. O. Roos, B. Schimmelpfennig, *Chem. Phys. Lett.* **2002**, *357*, 230-240; e) J. Paulovic, T. Nakajima, K. Hirao, R. Lindh, P. A. Malmqvist, *J. Chem. Phys.* **2003**, *119*, 798-805; f) B. O. Roos, P. A. Malmqvist, *Phys. Chem. Chem. Phys.* **2004**, *6*, 2919-2927.

[4] P. A. Malmqvist, B. O. Roos, *Chem. Phys. Lett.* **1989**, *155*, 189-194.

[5] a) B. O. Roos, K. Andersson, M. P. Fulscher, P. A. Malmqvist, L. SerranoAndres, K. Pierloot, M. Merchan, *Adv. Chem. Phys.* **1996**, *93*, 219-331; b) J. Finley, P.-Å. Malmqvist, B. O. Roos, L. Serrano-Andrés, *Chem. Phys. Lett.* **1998**, *288*, 299; c) G. Ghigo, B. O. Roos, P. A. Malmqvist, *Chem. Phys. Lett.* **2004**, *396*, 142-149; d) S. Vancoillie, M. G. Delcey, R. Lindh, V. Vysotskiy, P. A. Malmqvist, V. Veryazov, *J. Comput. Chem.* **2013**, *34*, 1937-1948.

[6] F. Neese, *Wires Comput. Mol. Sci.* **2018**, *8*.

[7] F. Weigend, R. Ahlrichs, *Phys. Chem. Chem. Phys.* **2005**, *7*, 3297-3305.

[8] S. Grimme, S. Ehrlich, L. Goerigk, *J. Comput. Chem.* **2011**, *32*, 1456-1465.

[9] L. Ungur, L. F. Chibotaru, *Phys. Chem. Chem. Phys.* **2011**, *13*, 20086-20090.

[10] a) A. N. Kulikov, L. A. Kaledin, A. I. Kobyliansky, L. V. Gurvich, *Can. J. Phys.* **1984**, *62*, 1855-1870; b) C. Linton, D. M. Gaudet, H. Schall, *J. Mol. Spectrosc.* **1986**, *115*, 58-73; c) Y. C. Liu, C. Linton, H. Schall, R. W. Field, *J. Mol. Spectrosc.* **1984**, *104*, 72-88.

[11] D. A. Varshalovich, A. N. Moskalev, and V. K. Khersonskii, Quantum Theory of Angular Momentum (World Scientific,Singapore, 1988).

[12] B. R. Judd, Second Quantization and Atomic Spectroscopy (The Johns Hopkins Press, Baltimore, 1967).

[13] C. W. Nielson and G. F. Koster, Spectroscopic Coefficients for the p^n, d^n, and f^n Configurations (MIT Press, Cambridge, 1963).